Photoinduced electron transfer and geminate recombination for photoexcited acceptors in a pure donor solvent

V. O. Saik, A. A. Goun, and M. D. Fayer[a)]
Department of Chemistry, Stanford University, Stanford, California 94305

(Received 29 January 2004; accepted 2 March 2004)

Photoinduced electron transfer and geminate recombination are studied for the systems rhodamine 3B ($R3B^+$) and rhodamine 6G ($R6G^+$), which are cations, in neat neutral *N*,*N*-dimethylaniline (DMA). Following photoexcitation of $R3B^+$ or $R6G^+$ (abbreviated as R^+), an electron is transferred from DMA to give the neutral radical R and the cation DMA^+. Because the DMA hole acceptor is the neat solvent, the forward transfer rate is very large, $\sim 5\times 10^{12}$ s^{-1}. The forward transfer is followed by geminate recombination, which displays a long-lived component suggesting several percent of the radicals escape geminate recombination. Spectrally resolved pump–probe experiments are used in which the probe is a ''white'' light continuum, and the full time-dependent spectrum is recorded with a spectrometer/charge-coupled device. Observations of stimulated emission (excited state decay—forward electron transfer), the R neutral radical spectrum, and the DMA^+ radical cation spectrum as well as the ground-state bleach recovery (geminate recombination) make it possible to unambiguously follow the electron transfer kinetics. Theoretical modeling shows that the long-lived component can be explained without invoking hole hopping or spin-forbidden transitions. © *2004 American Institute of Physics.* [DOI: 10.1063/1.1712826]

I. INTRODUCTION

Liquids are an important medium for electron transfer processes. In spite of the ubiquity of liquids, understanding photoinduced electron transfer between donors and acceptors in liquids remains a challenging problem. In many photoinduced electron transfer experiments,[1–3] a low concentration donor ($<10^{-4}$ M) and high concentration acceptors ($\sim$0.1 M) are dissolved in a liquid solvent. The time dependence of photoinduced electron transfer is determined by the distance dependence of the intermolecular interactions, which in turn is controlled by the strength of the electronic interaction, the free-energy change upon electron transfer, and the reorganization energy.[4–9] Because the particles are constantly moving through the liquid, their relative positions, and therefore, the transfer rates, and not fixed. The transfer rate from a particular donor to the collection of acceptors is a complex time-dependent function.[3,10–14]

Following forward electron transfer, geminate recombination (electron–hole recombination) can occur.[12–15] The time-dependent concentration of radicals produced by forward electron transfer depends on the relative rates of forward transfer and geminate recombination. Because the species prior to and following electron transfer are not the same, the distance-dependent forward and back transfer rates, in general, are not the same.[14] Furthermore, for donors and acceptors in a liquid solvent, there is a wide distribution of initial donor/acceptor separations. For a donor without an acceptor nearby at the time of photoexcitation, diffusion is required to bring an acceptor sufficiently close to permit electron transfer to occur.[3,10–14] A competition exists between geminate recombination and the escape of the radicals from the immediate vicinity of their generation. Because electron transfer is short range ($<\sim$10 Å), separation of the radicals over relatively short distances can lead to the generation of long-lived radicals.

Another scenario for electron transfer in liquids occurs when a low concentration acceptor is dissolved in a pure liquid that acts as the electron donor.[16,17] With the donors surrounding the acceptor, photoexcitation of the acceptor leads to very rapid electron transfer. Forward electron transfer has been studied in considerable detail in pure electron donor liquids with the emphasis on understanding the donor/acceptor electronic coupling matrix element.[16] Some attention has be paid to events following forward electron transfer using single-color nonlinear spectroscopic techniques.[17]

In this paper, photoinduced electron transfer and back transfer (geminate recombination) are studied in a pure donor liquid using spectrally resolved pump–probe experiments. The systems are rhodamine3B ($R3B^+$) and rhodamine6G ($R6G^+$), which are cations, in neat neutral *N*,*N*-dimethylaniline (DMA). $R3B^+$ is the ethylester of rhodamine B, which is a carboxylic acid.[18] Following photoexcitation of $R3B^+$ or $R6G^+$ an electron is transferred from DMA to give the neutral radical R and the cation DMA^+. A great deal of experimental and theoretical work has been done in a number of solvents on $R3B^+$/DMA in which DMA is in relatively low concentration.[3] In the theoretical treatments used to describe electron transfer in solution,[3,10,14,19] the species that is in very low concentration and is photoexcited is called the donor. Because $R3B^+$ or $R6G^+$ are hole donors, we will refer to them as the donors and DMA as the hole acceptor.

In the experiments a short pump pulse ($\sim$100 fs) is used to excite $R3B^+$ or $R6G^+$ at 565 nm. A ''white'' light con-

a)Electronic mail: fayer@stanford.edu

tinuum is then used to take the full spectrum from 380 to 650 nm. The spectrum is observed with a monochromator and a CCD camera. By observing the entire spectrum as a function of time, it is possible to examine the dynamics of different features in the spectrum that are not observable in a single-color experiment.[17] The time dependence of the ground-state bleach, the excited state population, and of particular importance, the neutral R3B and R6G radicals formed by forward electron transfer and the DMA^+ radical cation, can be independently investigated.

II. EXPERIMENTAL PROCEDURES

Pump–probe experiments in which a particular wavelength is used for the pump and a continuum is used as the probe were performed using a Ti:Sapphire regenerative amplified source, and optical parametric amplifier (OPA) and either CCD detection system (broadband detection) or a lock-in amplifier system (narrow-band detection). A double-pass BBO OPA pumped by the output of the Ti:Sapphire regenerative amplifier (800 nm, ~85 fs) was used to make 1.9 μm light. The leftover 800 nm pulses were then summed with the ~1.9 μm pulses in another BBO crystal to produce the 565 nm pump pulses at a repetition rate of 1 kHz. This wavelength is on the red side of the $R3B^+$ and $R6G^+$ absorption spectra. The intensity of pump light was attenuated using a half-wave plate and polarizer combination. The pump energy (0.3–0.4 μJ/pulse) was chosen to make sure that the signal was linear in the pump intensity and that there was no sample degradation. All measurements described here were performed at the magic angle between the pump and probe beams unless otherwise specified.

A white light continuum, used for the probe, was generated by focusing 1–2 μJ of 800 nm light onto the back surface of a rotating CaF_2 crystal. A half-wave plate/polarizer combination was used to attenuate the 800 nm to give the most stable white light. Rotation was necessary to avoid rapid damage to the CaF_2. Use of CaF_2 with the 800 nm pump permitted continuum to be generated from the near IR to somewhat beyond 380 nm. The white light was separated into two beams by a beam splitter. One beam was used as the probe crossed with the pump in the sample, and the other one, which passed through an unpumped spot in the sample, was used as a reference to monitor the intensity and spectral characteristics of the white light. Probe and reference beams were collimated and then focused into the sample. The pump and probe beams had the spot sizes of about 100 and 50 μm, respectively. The delay between the pump and probe was achieved by passing the pump beam down two delay lines, a high-resolution delay with ~1 fs resolution and a long low-resolution delay (~1 ps) that produced a maximum delay of ~12 ns.

The probe and the reference beams, after passing through the sample, were focused into two optical fibers by two microscope objectives. The outputs of the fibers are at the entrance slit of a 0.3 m monochromator with a 300 line/mm. The dispersed outputs of the two input beams are detected by a 1340×100 pixel CCD detector. The probe and the reference produce separately readout stripes on the CCD, which are used to obtain the difference absorption spectrum between pump on and pump off. The reference spectrum permits correction for variation over time of the white light characteristics. Comparing the spectrum with the pump on and the pump off determined absolute differences in absorbance.

In an alternative detection configuration, the probe and reference beams were directed out of an exit slit on the monochromator rather than into the CCD. Two photomultiplier tubes (PMT) were used after the exit slit to measure the probe and reference signals at a selected wavelength. Two gated integrators obtained signals from the PMTs, and the probe signal was divided by reference signal, the log taken using an analog processor. The ratio was fed to a lock-in amplifier that detected the signal at 500 Hz. A mechanical chopper blocked every other pump pulse, resulting in a difference signal at 500 Hz.

Time resolution of the system, that is the cross correlation between the pump pulse and the white light probe pulse, was determined by fitting the rising edge of the pump–probe signal of $R3B^+$ in ethanol solution to be ~200 fs. The shift in the position of the rising edge as a function of wavelength was used to determine the influence of chirp of the white light on the time dependence measured at different wavelengths.

All data were taken at room temperature, 21 °C. The cells were made of fused silica and had a 1 mm path length. Each sample contained 0.05 mM $R3B^+$ or $R6G^+$ (Exciton). DMA (Aldrich, 99.5+%) was used as received. Samples were degassed by several freeze–pump–thaw cycles and sealed under vacuum. All samples were stored in the dark. No measurable change in the absorption spectra and the transient spectra were observed over the period of the experimental measurements.

III. RESULTS AND DISCUSSION

Features associated with the $R3B^+$ spectrum and the R3B neutral radical spectrum can be identified by examining $R3B^+$ in a nonparticipating solvent without and with DMA in the same solvent. Figure 1 displays three pump–probe difference spectra taken with the CCD. The solvent is propylene glycol and the probe delay is 8 ps. The solid curve is for $R3B^+$ taken with no DMA in the solution. The negative-going peak at ~570 nm is the ground-state bleach. The positive-going peak at ~445 nm is an excited state–excited state absorption. The broad, low amplitude negative-going feature to the red of ~600 nm is stimulated emission induced by the probe. Measurements of standard absorption and fluorescence spectra show that the peak of the stimulated emission (fluorescence) is at ~590 nm. At this wavelength there is overlap between the absorption and the emission. By 600 nm the absorption has fallen to zero.[18] Therefore, measurements presented below at 620 nm do not contain any contribution from the ground-state bleach. $R3B^+$ solutions in several solvents without DMA acceptors show the same features.[20] The dashed curve in Fig. 1 shows the spectrum with a DMA acceptor concentration of 0.3 M. A new feature is evident at ~430 nm. This feature arises from the generation of the R3B neutral radical via electron transfer from a DMA.[21] The region of stimulated emission, which reflects

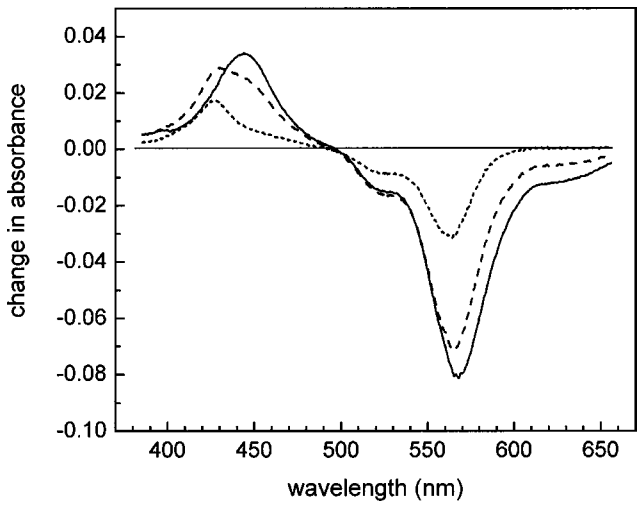

FIG. 1. Pump–probe difference spectra at 8 ps delay in propylene glycol. The solid curve is $R3B^+$ taken with no DMA acceptors. The dashed curve is the spectrum with a DMA acceptor concentration of 0.3 M. A new feature at ~430 nm arises from the generation of the R3B neutral radical via electron transfer from a DMA. The dotted curve results from subtracting the solid curve from the dashed curve. The R3B neutral radical spectrum is the peak at 430 nm.

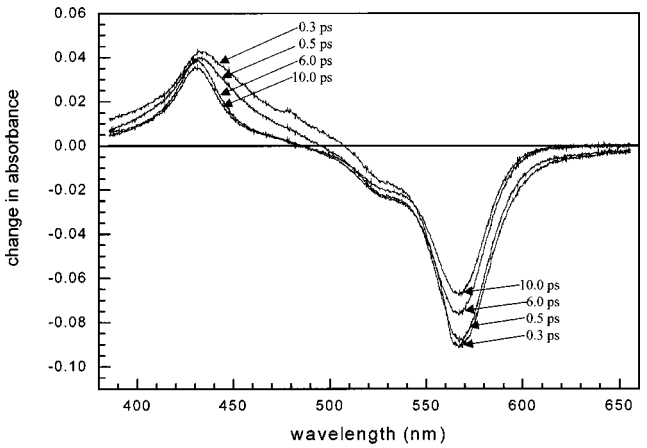

FIG. 2. Pump–probe difference spectra of $R3B^+$ in pure DMA taken at four different times. By ~6 ps, the peak at 430 nm is the R3B neutral radical absorption.

the $R3B^+$ excited state population, has decreased by ~50%. However, the ground-state bleach has decreased much less. Forward electron transfer quenches the excited state population, but the ground-state bleach does not recover until electron back transfer has occurred to regenerate $R3B^+$.

To obtain a spectrum of the R3B neutral radical, it is necessary to subtract the excited state–excited state absorption band. The excited state–excited state absorption has amplitude that is proportional to the stimulated emission band because they are both determined by the number of excited states. Therefore, the R3B spectrum is obtained by subtracting the no-acceptor spectrum (solid curve) from the spectrum with acceptors (dashed curve) after scaling it to the spectrum with acceptors in the region of the stimulated emission. The resulting spectrum (dotted curve) shows the R3B neutral radical in the region around ~430 nm. This spectrum coincides with the spectrum of $R3B^+$ taken using pulsed radiolysis to produce the R3B neutral radical.[21] We can estimate the extinction coefficient of the R3B neutral radical by comparing the amplitude of the signal at 430 nm to that of the ground-state bleach at 564 nm. The result is $\sim 3\times 10^4$ $M^{-1}\,cm^{-1}$, which is close to the reported value. We were unable to observe the DMA^+ absorption in the solution. From the literature it is known that it is peaked at 470 nm with a maximum extinction coefficient of ~4700 $M^{-1}\,cm^{-1}$.[22,23] In the dotted spectrum in Fig. 1, the DMA^+ would have an absorbance of ~0.001, and would be obscured by the R3B neutral radical absorption. However, observation of the tail of the DMA^+ spectrum in the pure DMA solvent is discussed below.

Figure 2 shows pump–probe difference spectra of $R3B^+$ in pure DMA taken at four different times. Because the solvent is composed of pure DMA hole acceptors, electron transfer is extremely fast. In Fig. 1, where the DMA is in moderate concentration, at 8 ps the R3B neutral radical (430 nm) is a large shoulder on the side of the $R3B^+$ excited state–excited state absorption peak (445 nm). In Fig. 2, in both the 6 and 10 ps spectra, there is no contribution from the $R3B^+$ excited state–excited state absorption peak. Even in the 0.3 ps spectrum in pure DMA (Fig. 2), the $R3B^+$ excited state–excited state absorption peak is only a shoulder on the side of the R3B neutral radical peak. By 0.5 ps, the contribution from the $R3B^+$ excited state–excited state absorption has shown a further substantial decrease. The $R3B^+$ excited state–excited state absorption is decreased as forward electron transfer depopulates the initially prepared $R3B^+$ excited state. By 6 ps, forward electron transfer is almost complete, and between 6 and 10 ps, back transfer has begun to reduce the R3B neutral radical peak at 430 nm. The features in the spectra to the red of 550 nm can be understood in a similar manner. In the short time spectra (0.3 and 0.5 ps) there is a nonzero tail to the red of 600 nm. This arises from simulated emission, which requires excited state population. By 6 ps, virtually all of the excited state population has decayed because of forward electron transfer. The lifetime of the $R3B^+$ excited state in the absence of electron transfer is ~2 ns, with some dependence on the solvent.[20] In the DMA solvent, the excited state population decay is completely dominated by forward electron transfer. There is some contribution to the negative-going peak at ~570 nm (mainly due to bleaching of the ground state) from overlap with the stimulated emission band. This was determined from the overlap of the absorption spectrum and the fluorescence spectrum.

While the forward electron transfer is extremely fast, and complete in a few ps (see below), the back electron transfer (geminate recombination) is substantially slower. By 6 ps, the peak at 430 nm arises solely from the R3B neutral radical generated by forward electron transfer. The negative peak at ~570 nm is caused solely by the ground-state bleach. Between 6 and 10 ps, these peaks begin to decay because of back electron transfer. Figure 3 is a schematic of the energy states and the kinetics. The system begins in the ground state (R^+-DMA) and is photoexcited to R^+*-DMA. The system can return to the ground state without electron transfer with a

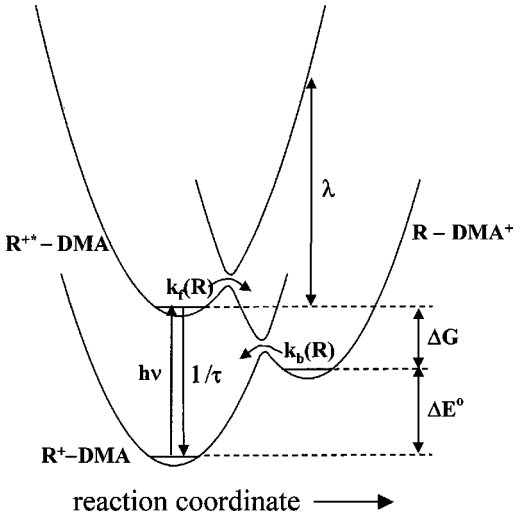

FIG. 3. Schematic of the energy states and the kinetics.

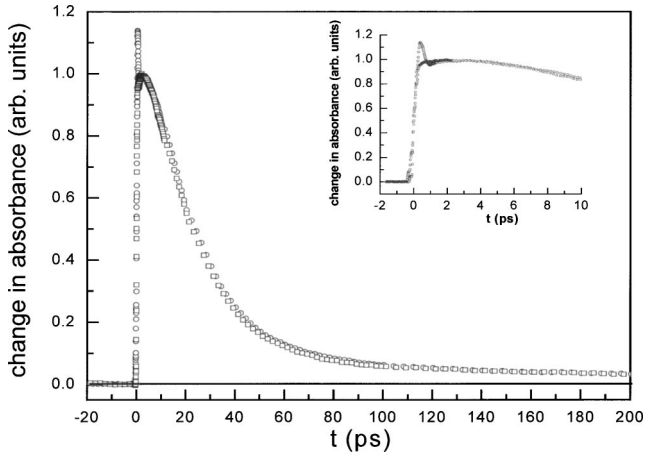

FIG. 4. Data at 540 nm (ground-state bleach, squares) and at 430 nm (circles), which after the first few ps are exclusively the R3B neutral radical. For short time at 430 nm there is a contribution from $R3B^+$* excited state–excited state absorption. The inset shows the same data on an expanded scale. The 540 nm data have been inverted. The decay of the R3B neutral radical via electron back transfer and the recovery of the ground-state bleach are identical.

rate $1/\tau$, where τ is the lifetime measured in the absence of electron transfer. Forward electron transfer can take place with the distance-dependent forward rate $k_f(R)$ to the charge transfer state, R-DMA^+. The system can return to the ground state via back electron transfer from the charge transfer state R-DMA^+ to R^+-DMA with the distance-dependent back transfer rate $k_b(R)$. The dynamics of the coupled problem of forward transfer and back transfer in solution have been discussed theoretically in detail.[12–15,24,25] The theory will be applied to analyze the data below. The free-energy difference between the ground state and the charge transfer state is the difference in donor/acceptor redox potentials, ΔE^o. The free-energy difference between the excited state and the charge transfer state is ΔG, the free energy associated with the forward electron transfer. λ is the reorganization energy. For electron transfer in the normal region $(-\Delta G<\lambda)$, a widely used form of $k(r)$ was developed by Marcus.[4–9] For the forward transfer, the Marcus form of the transfer rate is employed. The back transfer is in the inverted regime, and the distance-dependent back transfer rate is modeled as an exponential.

Figure 4 shows details of the dynamics at two wavelengths, 430 nm (circles) and 540 nm (squares). The inset shows that same data with an expanded time scale. The data at 540 nm is the ground-state bleach. These data, which are negative going (see Fig. 2), has been inverted for comparison with the 430 nm data. The 540 nm data are on the blue side of the bleach spectrum to avoid any possible contamination from simulated emission. Equivalent data were also taken at 560 nm, near the peak of the bleach. They are identical to the data taken at 540 nm. At short times (<a few ps), the data at 430 nm are a combination of excited state–excited state absorption of $R3B^+$ and absorption by the neutral R3B radical. As the initially excited $R3B^+$ is converted to R3B by electron transfer, the excited state–excited state absorption peak decays and the neutral radical peak grows in (see the band shapes in Fig. 1). The extinction coefficient for the $R3B^+$ excited state–excited state absorption is slightly larger at 430 nm than the R3B neutral radical extinction coefficient. Therefore, at 430 nm, the signal initially displays a small rapid drop as the very fast forward electron transfer occurs. In the inset, it can be seen that the signal actually decays rapidly and then shows a small rise at ~1 ps because of the difference in extinction coefficients.

Following the first few ps (see below), forward electron transfer is virtually complete, and the signal at 430 nm arises solely from the R3B neutral radicals. The signal then decays because of electron back transfer. The 540 nm data are the inverted ground-state bleach. The bleach is created immediately upon excitation and decays only with the repopulation of the ground state. As shown in Fig. 3, this can occur through excited state population relaxation and electron back transfer. However, because the excited state lifetime (~2 ns) is so long relative to the time scales under consideration, population relaxation can be neglected, and the 540 nm decay caused completely by electron back transfer. As can be seen in the main part of Fig. 4 and in the inset, after ~2 ps, the decay of the R3B neutral radical absorption (430 nm) and the decay of the ground-state bleach (540 nm) are identical. The identical behavior of the neutral radical absorption and the bleach is consistent with the model shown qualitatively in Fig. 3 and which will be used in detailed calculations below. As is clear from the data in Fig. 4, forward transfer is much faster than the back transfer. The decay of the bulk of both back transfer signals can be characterized by an ~25 ps exponential. However, even at relatively short times, the decay is not strictly exponential, and it does not decay exponentially to zero. The data have a very long tail that decays increasingly slowly as time goes on. The nonexponential decay and the long tail will be reproduced below using the statistical mechanical theory of forward transfer and geminate recombination.[12–15,24,25]

Figure 5 displays data taken at 620 nm. The inset shows the same data with an expanded time scale. The data have been inverted. As discussed in connection with Fig. 1, the signal at 620 nm is dominated by stimulated emission from the excited donors $R3B^+$*. Electron transfer converts

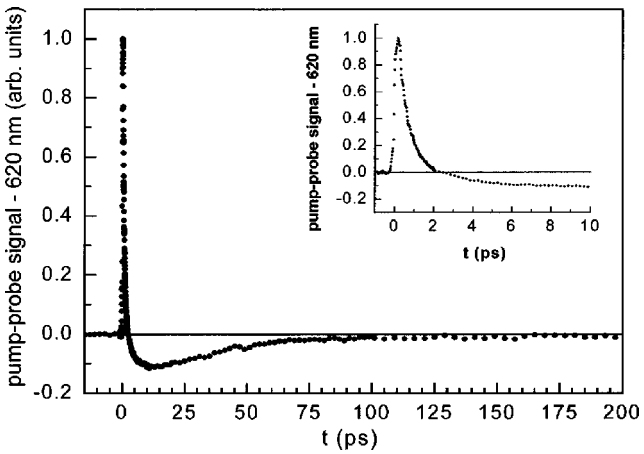

FIG. 5. Data at 620 nm. At short time ($<\sim 2$ ps) the data are dominated by stimulated emission from the initially excited state, $R3B^{+}*$. The decay reflects forward electron transfer. A weak absorption at 620 nm from the DMA^{+} radical cation contributes to the signal at longer time. For $t>\sim 20$ ps, the signal is the decay of the DMA^{+} caused by electron back transfer. The inset is the same data on an expanded time scale.

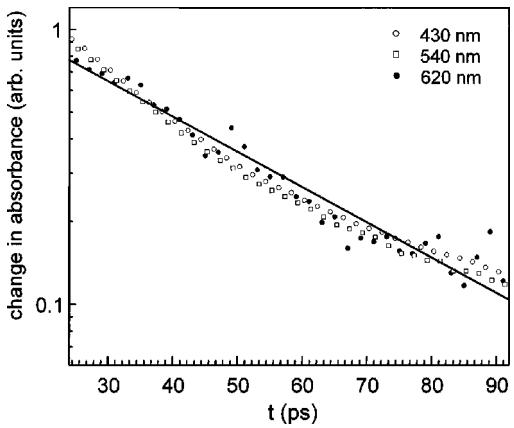

FIG. 6. Semilog plot of data at 430 nm (R3B neutral radical, open circles), 540 nm (ground-state bleach, squares), and 620 nm (DMA^{+} radical cation, filled circles) for $t>25$ ps. The data show that the decays of the radicals via electron back transfer and the decay of the ground-state bleach have identical time dependences. The line illustrates that the decays are not exponential.

$R3B^{+}*$ to ground-state R3B neutral radicals and eliminates the stimulated emission. The forward electron transfer that eliminates the $R3B^{+}*$ species is extremely fast and nonexponential. The main decay of signal from ~ 0.5 to ~ 1.5 ps can be approximately characterized by an exponential decay with decay time of ~ 0.5 ps. However, the peak amplitude of the signal, which was normalized, is reduced substantially by the convolution with the instrument response (200 fs).

An obvious feature of the data is that they dip below zero, and then recover, decaying toward zero as t approaches 200 ps. The form of the data can be understood by careful consideration of all of the species that contribute to the spectra displayed in Figs. 1 and 2. From the literature, the spectrum and the peak extinction coefficient of the DMA radical cation (DMA^{+}) are known.[22,23] DMA^{+} has a very weak tail that extends past 620 nm. From the spectrum, the extinction coefficient at 620 nm was approximately determined. The absorption spectrum and the fluorescence spectrum of $R3B^{+}$ were measured, and the extinction coefficient of $R3B^{+}$ was determined. The absorption spectrum and its maximum extinction coefficient, as well as the fluorescence spectrum, are virtually identical to rhodamine B.[18] In addition, we measured the transient absorption spectrum of $R3B^{+}$ in solution without DMA (see Fig. 1) and the fluorescence spectrum using the spectrum/CCD instrument under identical conditions. This permitted the ''effective stimulated emission extinction coefficient'' to be determined by comparison to the bleach spectrum. (The Einstein B coefficient for absorption is equal to the Einstein B coefficient for simulated emission.[26] The effective stimulated emission extinction coefficient is equivalent to the Einstein B coefficient for simulated emission.) Using the DMA^{+} extinction coefficient at 620 nm and the $R3B^{+}$ effective stimulated emission extinction coefficient at 620 nm, their ratio was determined. At 620 nm, the $R3B^{+}$ stimulated emission is ~ 70 times stronger than the DMA^{+} transient absorption if the two species had the same concentration.

In Fig. 5 around $t=\sim 0$ there are far more $R3B^{+}*$ (excited states) than DMA^{+} radicals, which gives rise to the large positive peak (increase in light transmitted through the sample). The number of excited states decays rapidly due to forward electron transfer. For the first portion of the decay, the signal essentially reflects the rate of forward electron transfer because the $R3B^{+}*$ stimulated emission is so much stronger than the DMA^{+} absorption. Even when the number of excited states is down to 2%, the ratio of the extinction coefficients will yield a positive signal in Fig. 5. However, once the $R3B^{+}*$ concentration becomes small enough and the DMA^{+} concentration becomes large enough, the signal will go negative because the DMA^{+} absorption (decrease in 620 nm probe transmission) will be greater than the $R3B^{+}*$ stimulated emission (increase in 620 nm probe transmission). The inset shows that for time past 10 ps, the signal is still becoming more negative. The main body of the figure shows that there is a turnaround between 10 and 15 ps. The broad nature of the turnaround is in part due to the disparities in the $R3B^{+}*$ effective stimulated emission extinction coefficient and the DMA^{+} absorption extinction coefficient. After ~ 25 ps, there is no contribution to the signal from $R3B^{+}*$. The signal arises solely from the DMA^{+} radical cations formed by forward electron transfer. Electron back transfer is responsible for the decay toward zero.

The discussions presented above state that following forward electron transfer, all of the dynamics observed arise from electron back transfer. Electron back transfer is measured by examining the time dependence of three different observables, the decay of the R3B neutral radical spectrum (430 nm), the reformation of $R3B^{+}$ measured by the decay of the ground-state bleach at 540 and 560 nm (not shown), and the decay of the DMA^{+} radical cation (620 nm). In Fig. 4, it can be seen that the decays at 430 and 540 nm are identical. In Fig. 6, the data for all three species are presented on a log plot. The data cover the range of 25 to 90 ps, which is after the turnover is complete in Fig. 5 and before the signal becomes too small to be useful. Because of the small

size of the DMA^+ extinction coefficient at 620 nm, the signal is weak and relatively noisy. Nonetheless, it is apparent from Fig. 6, that all three species exhibit the identical decays within experimental error. The line in Fig. 6 reflects an exponential decay. Clearly, the three data sets exhibit nonexponential decays.

IV. THEORETICAL MODELING

The model system for photoinduced intermolecular electron transfer followed by back transfer (geminate recombination) in liquids has been described in detail previously.[10,19] The theory was derived for donors and acceptors in a solvent. The donors, as in this study, are very low in concentration. However, in the theory, the acceptors were taken to be in *moderate to low concentration* to avoid the problem of acceptor–acceptor excluded volume affects in the spatial averaging procedure.[27] Here, the ''solvent'' is composed of pure DMA acceptors. The influence of the acceptor–acceptor excluded volume on the calculations will be discussed qualitatively after presentation of the results.

Upon photoexcitation, the donors can undergo forward electron transfer to one of the many acceptors in solution. In relatively dilute solution, which acceptor receives the electron depends on the spatial distribution of acceptors about the excited donor and on molecular diffusion in the liquid. While the theoretical treatment is general for any initial charges on the donors and acceptors, in the experiments described here, there are no ionic Coulomb interactions between the donor and acceptors before or after electron transfer. Therefore, the Coulomb term in the theory is set to zero. In the most likely scenario, the electron will back transfer from DMA^+ to R3B, regenerating the ground state. Because the concentration of donors is low, only geminate recombination is considered. Diffusion can separate the radical formed by forward transfer, giving rise to long-lived radicals. Another possibility is that hole hopping could occur between DMA^+ and DMA. This is not considered in the theory because it is energetically unfavorable, and the data can be explained strictly through geminate recombination and diffusion. Processes that regenerate the donor excited state are also energetically unfavorable for the systems studied here and are assumed to be negligible. Comparisons of the experimental results to the calculations presented below indicate that the formation of triplet state radical pairs is not involved in the kinetics. The three-level system (consisting only of ground states, excited donor states, and radical states) is shown schematically in Fig. 3.

The goal of the theory is to permit calculation of the physical observables: the state survival probabilities $\langle P_{ex}(t)\rangle$ and $\langle P_{ct}(t)\rangle$. If the donor is photoexcited at time 0, then $\langle P_{ex}(t)\rangle$ is the probability that the donor is still excited at some later time t, while $\langle P_{ct}(t)\rangle$ is the time-dependent probability that the radicals formed by forward transfer still exist. As time evolves, the probability of the donor remaining excited, $\langle P_{ex}(t)\rangle$, decays due to forward electron transfer. While $\langle P_{ex}(t)\rangle$ decays from a value of 1.0 (unit probability at time 0), $\langle P_{ct}(t)\rangle$, the probability of finding the donor and acceptor in their radical states, builds up from 0 as forward transfer occurs and then decays as back transfer acts to deplete the radical population. The ensemble averaging techniques relate the observables to the two particle survival probabilities. For the forward transfer, $\langle P_{ex}(t)\rangle$ has been derived in detail.[10,11] The result is

$$\langle P_{ex}(t)\rangle = \exp(-t/\tau)\exp\left(-4\pi C\int_{R_m}^{\infty}[1-S_{ex}(t|R_0)]\times R_0^2 g(R_0)\,dR_0\right). \quad (1)$$

Here, τ, C, and R_m denote, respectively, the donor ($R3B^+$) lifetime in the absence of acceptors, the acceptor concentration, and the donor–acceptor contact distance (sum of their radii). $g(R_0)$ is an appropriate donor/acceptor radial distribution function. $S_{ex}(t|R_0)$ is the two-particle excited-state survival probability, a theoretical construct for a hypothetical system in which there is one donor and only one acceptor. Given that the acceptor is at distance R_0 from the donor at time 0, $S_{ex}(t|R_0)$ is the probability that the donor is still excited at time t later. $S_{ex}(t|R_0)$ satisfies the well-known differential equation, with associated initial condition, and reflecting boundary condition at contact[14,28]

$$\frac{\partial}{\partial t}S_{ex}(t|R_0) = L^+_{R_0}S_{ex}(t|R_0) - k_f(R_0)S_{ex}(t|R_0),$$

$$S_{ex}(0|R_0) = 1, \quad (2)$$

$$4\pi R_0^2\frac{\partial}{\partial R_0}S_{ex}(t|R_0)\Big|_{R_0=R_m} = 0,$$

where $k_f(R_0)$ is a distance-dependent forward transfer rate, the specification of which is given below. $L^+_{R_0}$ is the adjoint of the Smoluchowski operator[28,29]

$$L^+_{R_0} = \frac{1}{R_0^2}\exp(V(R_0))\frac{\partial}{\partial R_0}D(R_0)R_0^2\exp(-V(R_0))\frac{\partial}{\partial R_0}, \quad (3)$$

where $V(R_0)$ is the potential divided by k_BT, and $D(R_0)$ is the distance-dependent diffusion constant (hydrodynamic effect).[10,14,19,30–32] Numerical evaluation of Eq. (2) can be followed by integration according to Eq. (1) to give the forward transfer experimental observable. This observable can be directly compared to experimental measurements of the time dependence of donor stimulated emission at 620 nm.

The inclusion of solvent structure and of a distance-dependent diffusion constant (hydrodynamic effect) in Eqs. (1)–(3) has been discussed previously.[10,14] The radial distribution function, $g(R_0)$, appears in both the spatial averaging and in the diffusional operator. In Eq. (3), the potential in the Smoluchowski operator includes the potential of mean force, that is, $V(R_0) = -\ln[g(R_0)]$. The distance dependence of the diffusion constant also appears in the Smoluchowski operator.

Derivation of $\langle P_{ct}(t)\rangle$ requires solving the coupled forward and back transfer problem. The techniques for performing the ensemble averages for the coupled problem have

been presented,[12,24,33] and solvent structure and hydrodynamic effects were included.[10,14] The result is

$$\langle P_{ct}(t)\rangle = 4\pi C \int_{R_m}^{\infty}\int_0^t S_{ct}(t-t'|R_0)k_f(R_0)S_{ex}(t'|R_0) \times\langle P_{ex}(t')\rangle dt' R_0^2 g(R_0) dR_0 . \quad (4)$$

$S_{ct}(t|R_0)$ is the two-particle survival probability for the radicals. Given that at time 0 the acceptor exists as a radical at R_0, $S_{ct}(t|R_0)$ is the probability that the donor and acceptor still exist as radicals at time t later, that is, back transfer has not yet occurred. $S_{ct}(t|R_0)$ can be calculated using Eq. (2) with the appropriate back transfer rate, $k_b(R_0)$.

Equation (4) represents the most commonly encountered experimental situation, in which the donor and acceptor have no Coulomb interaction prior to forward electron transfer. $S_{ct}(t|R_0)$ satisfies a differential equation equivalent to that of $S_{ex}(t|R_0)$. However, while the results briefly outlined above are formally correct for diffusion in a potential of mean force, inclusion of any additional potential in the forward transfer requires modification of the ion survival equations [Eq. (4)].[14] Furthermore, if the radicals produced by forward electron transfer have a Coulomb interaction, an additional Coulomb term in the potential for the back transfer is required.[14]

For the forward electron transfer, $k_f(R)$ is obtained using the well-known Marcus result[4,6]

$$k_f(R) = \frac{2\pi}{\hbar\sqrt{4\pi\lambda(R)k_B T}} J_{of}^2 \exp\left(\frac{-(\Delta G_f(R)+\lambda(R))^2}{4\pi(R)k_B T}\right) \times\exp(-\beta_f(R-R_m)), \quad (5a)$$

where

$$\lambda(R) = \frac{e^2}{4\pi\varepsilon_0}\left(\frac{1}{\varepsilon_{op}}-\frac{1}{\varepsilon_s}\right)\left(\frac{1}{R_d}+\frac{1}{R_a}-\frac{2}{R}\right). \quad (5b)$$

J_{of} is the electronic coupling matrix element between a donor and an acceptor at contact for forward transfer. $\Delta G_f(R)$ is the free-energy change for the forward transfer, obtained from the cyclic voltammetry experiments and the Rehm–Weller equation.[14,34,35] ε_{op} and ε_s are the optical and static dielectric constants of the solvent, ε_0 is the permittivity of free space, and R_d and R_a are the donor and acceptor radii, respectively (see Ref. 3). Equation (5a) is appropriate in the noninverted regime.[9] ΔG_f for $R3B^+$ and DMA have been reported in a number of solvents.[3] Since ΔG_f is relatively small for the forward transfer, Eq. (5a) is expected to be accurate. The adjustable parameters are then J_{of} and β_f, which determine the magnitude and distance dependence of the electronic coupling, respectively.

The back transfer is in the highly inverted regime, for which Eq. (5) is not appropriate. In the highly inverted regime, tunneling pathways become dominant, and quantum-mechanical treatments are available.[7,36–39] However, quantum-mechanical treatments require a large number of parameters, which, in general, are not known. In the absence of specific knowledge of the necessary parameters, a simpler exponential distance dependence appears to be able to provide information on the distance dependence of the transfer rate and the rate at contact. That is

$$k_b(R) = K\exp[\beta_b(R_m - R)]. \quad (6)$$

Equation (6) is equivalent to assuming that the distance dependence of the reorganization energy can be neglected. For the analysis presented below, which is intended to explicate the major features of the forward transfer and geminate recombination, but not to extract detailed parameters from the calculations, Eq. (6) is adequate.

The theory briefly outlined above requires a substantial number of input parameters, some of which are known and some are adjusted. For reasons discussed further below, the comparisons between the calculations and the data are only semiquantitative and are intended for heuristic purposes. The aim is to show that the basic features of the forward and back transfer data can be understood only in terms of the model pictured in Fig. 3. The theory calculates two observables, $P_{ex}(t)$ (the time-dependent excited state probability) and $P_{ct}(t)$ (the time-dependent charge transfer state probability). $P_{ex}(t)$ is obtained from the data at 620 nm (Fig. 5) with the contribution for the absorption of the DMA^+ radicals removed. At short time, the 620 nm data reflect $P_{ex}(t)$. The ground-state bleach data at 540 nm (see Figs. 4 and 6) is scaled to the long-time portion of the 620 nm data, which is due solely to DMA^+, and subtracted. The $P_{ct}(t)$ data are obtained from the R3B neutral radical data at 430 nm (Fig. 4) after the short-time contribution from excited state–excited state absorption is removed using the $P_{ex}(t)$ curve. The result is pure $P_{ex}(t)$ and $P_{ct}(t)$ curves without contributions from other species. This process will introduce a small amount of experimental uncertainty in the curves.

In the calculation, the following constants are employed. The static and optical dielectric constants of the liquid (DMA) are 5.01 and 2.43, respectively. The DMA viscosity is 1.29 cP.[40] The molecular radii of DMA and R3B are 0.275 and 0.412 nm, respectively.[3] Using the viscosity, the diameters, and the Stokes–Einstein equation, the mutual diffusion coefficient of DMA+R3B is 202.0 $Å^2$/ns. The ΔGs were determined from the redox potentials in acetonitrile.[3] The redox potentials were corrected for dielectric constant using the standard Weller equation.[3,41,42] This works very well when one high dielectric constant is converted to another high dielectric constant. There is considerably more error when measurements in a high dielectric constant (acetonitrile) are used to determine the redox potential in a low dielectric constant liquid like DMA. Therefore, there is some error in the ΔG values of $\Delta G_f = -0.294$ eV and $\Delta G_b = -1.894$ eV. Using Eq. (5b), the reorganization energy at contact, $\lambda = 0.5821$ eV. The normal region of electron transfer is taken to be $-\Delta G < \lambda$.[9] Therefore, the forward transfer is in the normal region and the back transfer is in the inverted region as mentioned above. To reduce the number of parameters further, β in Eq. (5a) we assume $\beta = Å^{-1}$ because β has been found to be ~ 1 $Å^{-1}$ in many studies.[7,38,43–45] In addition, previous electron transfer measurements on the donor and acceptor studied here indicate that $\beta \cong 1$ $Å^{-1}$.[3] We have also fixed $\beta = 1$ $Å^{-1}$ for the back

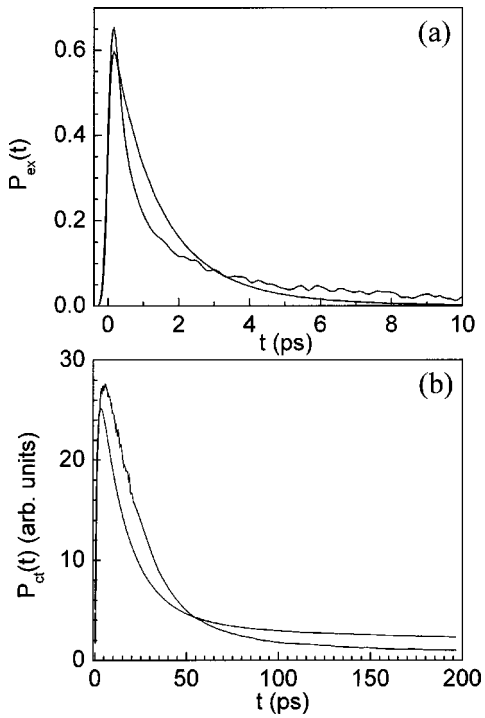

FIG. 7. (a) Decay of the excited state $R3B^{+}*$ [$P_{ex}(t)$] measured at 620 nm (stimulated emission signal with DMA^{+} absorption removed), and the theoretically calculated $P_{ex}(t)$ (see the text). (b) Decay of the R3B neutral radical [$P_{ct}(t)$] measured at 430 nm (short-time contribution from the $R3B^{+}*$ excited state–excited state absorption removed), and the theoretically calculated $P_{ct}(t)$ (see the text).

transfer [Eq. (6)]. That leaves only one adjustable parameter for the forward transfer, J_{of}, and one adjustable parameter for the back transfer, K.

Figures 7(a) and 7(b) display $P_{ex}(t)$ and $P_{ct}(t)$ along with calculated curves. The areas of the data curves and the calculated curves have been normalized. The value of $J_{of} = 50\ cm^{-1}$ and the value of $K = 100$. Both calculations reproduce the data reasonably well but certainly not quantitatively. The calculated $P_{ex}(t)$ decays too slowly at short time and then too rapidly at longer time. The decay of $P_{ct}(t)$ at short time is about right and, of most importance, the calculated $P_{ct}(t)$ displays the long tail observed in the data. However, the amplitude of the tail is too great. The long tail in the back transfer is initially somewhat surprising. Because many acceptors are in contact with the donor, it would be expected that forward transfer occurs to a contact neighbor followed by very rapid back transfer. However, the back transfer is in the highly inverted region, which slows it down considerably. The relatively slow back transfer distance-dependent rate constant permits diffusion to separate the radicals formed by forward transfer, giving rise to the long tail in $P_{ct}(t)$. It is unnecessary to invoke hole hopping from DMA^{+} to another DMA or the formation of a radical pair triplet state, leading to spin-forbidden back transfer to account for the data.

The theoretical calculations do not reproduce the data quantitatively. This is not surprising. The theory was developed for a donor interacting with relatively dilute acceptors, $<\sim 0.5$ M. Here, the acceptor is the pure liquid surrounding the donor. The theoretical development does not account for acceptor–acceptor excluded volume, which is unimportant for relatively low concentrations. In relatively dilute solution, interchanging an acceptor with an adjacent solvent molecule is a distinct configuration in the ensemble average. In pure DMA, interchanging a DMA with an adjacent DMA is not a distinct configuration. Therefore, in pure DMA, the theory overcounts configurations in the ensemble average. In an initial study of the $R3B^{+}$/DMA system in a number of dilute solutions, J_{of} was found to be $\sim 300\ cm^{-1}$.[3] In a more recent study with improved data that spanned a much wider range of times, very good agreement was obtained between the shapes of the decay curves and the calculations, and J_{of} was found to be $\sim 200\ cm^{-1}$.[20] If a value of $J_{of} = 200\ cm^{-1}$ is used in the calculations, $P_{ex}(t)$ decays much too fast. The reduction in J_{of} used to obtain the semiquantitative agreement shown in Fig. 7 is presumably due to the influence of acceptor–acceptor excluded volume. Reducing J_{of} slows the rate of electron transfer, which to some extent makes up for the inclusion of too many configurations in the ensemble average. However, changing J_{of} does not have the same affect on the shape of the curve as changing the distribution of spatial configurations of the acceptors. Therefore, reducing J_{of} slows the decay into the appropriate range but does not produce the completely correct shape.

The calculated $P_{ct}(t)$ in Fig. 7(b) has approximately the correct shape, but overestimates the amplitude of the long tail. A general feature of the calculations is that the long component does not decay to zero at infinite time. The amplitude of the tail at infinite time in the calculation is the fraction of radicals that escapes geminate recombination. In a real system, nongeminate recombination will eventually quench the radicals. From the experimental data, it is possible to estimate the fraction of radicals that escapes geminate recombination. For times longer than the 200 ps radical recombination data shown in Fig. 4, the long-time tail becomes increasing flat. By 600 ps (data not shown), the tail is flat within experimental error. From the amplitude of the tail, we estimate that the escape fraction for $R3B/DMA^{+}$ radicals is $\sim 3\%$.

Another factor that comes into play is the orientational dependence of the electronic coupling. A study of electron transfer between coumarin dyes in aromatic amine acceptors including DMA showed that there is a significant angular dependence to the electronic coupling matrix element.[16] In the theory used to analyze the data, the coupling does not have an angular dependence. For relatively dilute solutions of acceptors, in which there is a broad distribution of distances and diffusion plays a significant role, the averaging over distance and orientational relaxation diminish the importance of the orientational dependence of the dynamics.[46] In pure DMA, contact neighbors dominate transfer and the time scale of forward transfer is so fast that orientational averaging will not occur. Therefore, the lack of knowledge of the angular dependence of the electron transfer and not having an angular average in the theory may also contribute to the difference in shape of the calculated and experimental curves.

Experiments provide some evidence that there is an an-

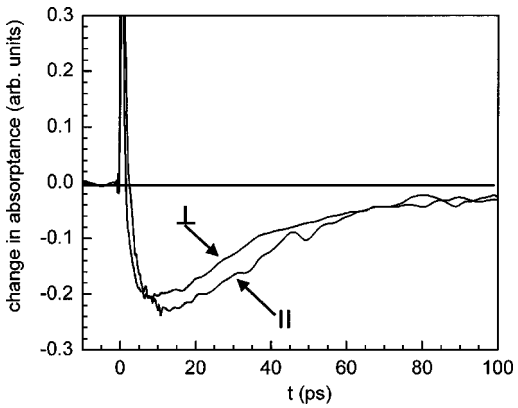

FIG. 8. Polarization selective data at 620 nm at longer times showing that the DMA^+ radical cation is created with an anisotropic distribution of orientations. Curve labeled ∥, pump and probe polarizations parallel. Curve labeled ⊥, pump and probe polarizations perpendicular.

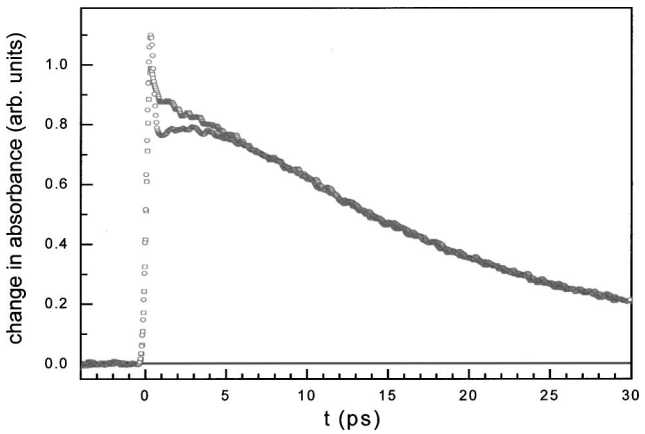

FIG. 9. $R6G^+$ data at 420 nm, which after ~5 ps are exclusively the R6G neutral radical (circles), and data taken at 540 nm, which is the ground-state bleach. The neutral radical, which decays via electron back transfer, and the recovery of the ground-state bleach are identical. Compare to Fig. 4, the equivalent data for $R3B^+$.

gular dependence to the transfer rate. Figure 8 shows curves taken at 620 nm with the pump polarization aligned parallel to and perpendicular to the probe polarization. In all of the previous data the pump polarization was at the magic angle relative to the probe polarization. In Fig. 8, following the decay of $R3B^+$* signal, the remaining DMA^+ signal shows a difference between the parallel and perpendicular polarizations. The difference vanishes in ~50 ps. Using the Debye–Stokes–Einstein equation for the orientational relaxation time and the viscosity and radius of DMA, orientational randomization should occur with a time constant of ~25 ps, which is consistent with the data. The observed difference between the parallel and perpendicular signals will only occur if the DMA^+ radicals formed by electron transfer are not produced with an isotropic distribution of orientations relative to the initially excited $R3B^+$*.

In a previous study of $R6G^+$ in DMA using single-color nonlinear optical experiments, the long-time portion of the data was attributed to vibrational cooling with a time constant of ~20 ps.[17] The single-color data assigned an electron back transfer time constant of 4 ps and a forward transfer time constant of 85 fs. We performed experiments on the $R6G^+$/DMA system that were identical to those described above. The time-dependent spectrum is almost the same as the one displayed in Fig. 2 for $R3B^+$/DMA except various features are shifted 10 to 20 nm to the blue. Figure 9 shows the decay of the R6G neutral radicals at 420 nm (circles) and the recovery of the ground-state bleach at 540 nm (squares). Figure 10 shows the decay at 610 nm of the $R6G^+$* stimulated emission (short-time positive signal) and the decay of the DMA^+ radical (long-time negative signal). Figures 9 and 10 should be compared to Figs. 4 and 5. The behavior of each curve is the same for the $R3B^+$ and $R6G^+$ donors, although the nonexponential decays vary somewhat in rate. As shown in Fig. 6, even the long-time (tens of ps) portions of the decays are not exponential. The previous experiments[17] did not spectrally identify the various species and follow their behavior independently, which apparently led to a misidentification of the decay processes.

To make a semiquantitative comparison between the dynamics measured for $R3B^+$ and $R6G^+$, the data from each system were fit with single exponentials: fits to the short-time portions of the stimulated emission curves (Figs. 5 and 10), which are measures of the forward transfer, and fits to the longer time portions of the neutral radical decay (Figs. 4 and 9), which are measures of the back transfer. The theoretical model employed in the analysis presented in Fig. 7 was not used. It is important to emphasize that the electron transfer processes are not exponential. As can be seen in Fig. 6, the neutral radical decay on the 20 ps time scale is not exponential, and by 200 ps (see Fig. 4) the decay is almost flat. By 600 ps (not shown), the neutral radical concentration is constant. Forward electron transfer is also nonexponential. The purpose of the single exponential fits is to permit a comparison of the data for the two rhodamines. Table I gives the approximate exponential constants obtained for the forward and back transfer as well as the estimated probability that the radicals escape geminate recombination.

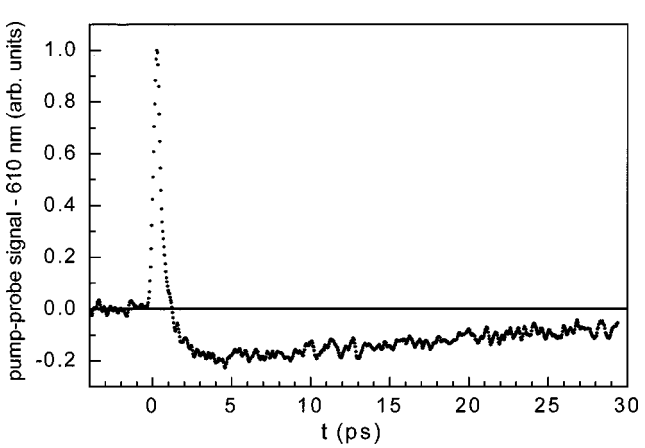

FIG. 10. $R6G^+$ data at 610 nm. At short time (<~1 ps) the data are dominated by stimulated emission from the initially excited state, $R6G^+$*. The decay reflects forward electron transfer. A weak absorption at 610 nm from the DMA^+ radical cation contributes to the signal at longer time. For $t > \sim 5$ ps, the signal is the decay of the DMA^+ caused by electron back transfer. Compare to Fig. 5, the equivalent data for $R3B^+$.

TABLE I. Single exponential approximations of the forward (f) and back (b) transfer times and estimated radical escape probability.

	τ_f (fs)[a]	τ_b (ps)[b]	P_{esc}
$R3B^+$ in DMA	500	25	0.03
$R6G^+$	260	22	0.02

[a]From the short-time decays of the stimulated emission (Figs. 5 and 10).
[b]From the intermediate time decays of the neutral radicals (Figs. 4 and 9).

The ~20 ps time scale processes, which become very slow at long times, are clearly identified as electron back transfer by observing the decay of the rhodamine neutral radicals, the recovery of the ground-state bleach, and the decay of the DMA^+ radicals. As seen in Figs. 4 and 6 ($R3B^+$/DMA) and Fig. 9 ($R6G^+$/DMA), the decays of the various species exhibit identical behavior. The forward electron transfer is monitored directly by observing the decay of the stimulated emission. The model calculations (Fig. 7) show that all of the dynamics can be accounted for through the processes of forward and back electron transfer as schematically illustrated in Fig. 3. By observing the spectroscopically identifiable species over a broad spectral range, it is possible to clearly assign the dynamics of the systems studied.

V. CONCLUDING REMARKS

Forward electron transfer and geminate recombination between excited rhodamine dyes, $R3B^+$ and $R6G^+$ (hole donors, R^+), in pure DMA (hole acceptor) were studied using time-resolved pump–probe spectroscopy over a broad range of wavelengths. By spectrally resolving the pump–probe data, the R^+ ground-state bleach, the $R^{+}*$ excited state–excited state absorption, the $R^{+}*$ stimulated emission, the R neutral radical, and the DMA^+ radical cation dynamics can all be explicated. Following optical excitation, $R^{+}*$ undergoes rapid electron transfer (hundreds of fs) in a nonexponential process, which generates the R neutral radical and the DMA^+ radical cation. The forward transfer process is in the normal regime of electron transfer.[9] As the radicals are formed, they immediately begin to geminately recombine. The electron back transfer (geminate recombination) is in the highly inverted regime[7,9,36–39] and is much slower than the forward transfer.

A statistical mechanics theory[10,19] was applied to the data to determine if the dynamics could be explained strictly in terms of forward and back electron transfer. The radicals formed by electron transfer display a long-lived component, and analysis shows that a few percent of the radicals escape geminate recombination in spite of the fact that forward electron transfer occurs almost exclusively between donors and acceptors that are in contact at $t=0$. The theory includes the liquid's radial distribution function and diffusion. However, the theory was developed for donors and acceptors in relatively dilute solution. Therefore, it does not account for acceptor–acceptor excluded volume, which means that at the high concentration of a solvent of pure electron donors, the theory overestimates the number of spatial configurations involved in the ensemble average. Therefore, the agreement between the calculations and the data is only semiquantitative. Nonetheless, the calculations account for all of the observed features, including the long-lived radicals. It is not necessary to invoke hole hopping or the formation of triplet radical pairs and spin-forbidden back transfer to understand the long-lived component of the radical population.

ACKNOWLEDGMENT

This work was supported by the Department of Energy (DE-FG03-84ER13251).

[1] L. Burel, M. Mostafavi, S. Murata, and M. Tachiya, J. Phys. Chem. A **103**, 5882 (1999).
[2] S. Murata, M. Nishimura, S. Y. Matsuzaki, and M. Tachiya, Chem. Phys. Lett. **219**, 200 (1994).
[3] H. L. Tavernier, M. M. Kalashnikov, and M. D. Fayer, J. Chem. Phys. **113**, 10191 (2000).
[4] R. A. Marcus, J. Chem. Phys. **24**, 966 (1956).
[5] R. A. Marcus, J. Chem. Phys. **24**, 979 (1956).
[6] R. A. Marcus, Annu. Rev. Phys. Chem. **15**, 155 (1964).
[7] R. A. Marcus and N. Sutin, Biochim. Biophys. Acta **811**, 265 (1985).
[8] N. Sutin, in *Electron Transfer in Inorganic, Organic, and Biological Systems*, edited by J. R. Bolton, N. Mataga, and G. McLendon (The American Chemical Society, Washington, 1991), p. 25.
[9] J. R. Bolton and M. D. Archer, in Ref. 8.
[10] S. F. Swallen, K. Weidemaier, and M. D. Fayer, J. Chem. Phys. **104**, 2976 (1996).
[11] M. Tachiya, Radiat. Phys. Chem. **21**, 167 (1983).
[12] Y. Lin, R. C. Dorfman, and M. D. Fayer, J. Chem. Phys. **90**, 159 (1989).
[13] R. C. Dorfman, Y. Lin, and M. D. Fayer, J. Phys. Chem. **94**, 8007 (1990).
[14] K. Weidemaier, H. L. Tavernier, S. F. Swallen, and M. D. Fayer, J. Phys. Chem. A **101**, 1887 (1997).
[15] K. Weidemaier and M. D. Fayer, J. Phys. Chem. **100**, 3767 (1996).
[16] E. W. Castner, D. Kennedy, and R. J. Cave, J. Phys. Chem. A **104**, 2869 (2000).
[17] Q.-H. Xu, G. D. Scholes, M. Yang, and G. R. Fleming, J. Phys. Chem. A **103**, 10348 (1999).
[18] I. B. Berlman, *Handbook of Fluorescence Spectra of Aromatic Molecules*, 2nd ed. (Academic, New York, 1971).
[19] S. F. Swallen, K. Weidemaier, H. L. Tavernier, and M. D. Fayer, J. Phys. Chem. **100**, 8106 (1996).
[20] V. Saik, A. Goun, J. Nanda, K. Shirota, H. L. Tavernier, and M. D. Fayer, J. Phys. Chem. (submitted).
[21] P. C. Beaumont, D. G. Johnson, and B. J. Parsons, J. Photochem. Photobiol., A **107**, 175 (1997).
[22] H. Kandori, K. Kemnitz, and K. Yoshihara, J. Phys. Chem. **96**, 8042 (1992).
[23] T. Shida, *Electronic Absorption Spectra of Radical Ions* (Elsevier, Amsterdam, 1988).
[24] A. I. Burshtein, Chem. Phys. Lett. **194**, 247 (1992).
[25] A. I. Burshtein, A. A. Zharikov, and N. V. Shokhirev, J. Chem. Phys. **96**, 1951 (1992).
[26] M. D. Fayer, *Elements of Quantum Mechanics* (Oxford University Press, New York, 2001).
[27] S. F. Swallen, K. Weidemaier, and M. D. Fayer, J. Phys. Chem. **99**, 1856 (1995).
[28] M. V. Smoluchowski, Z. Phys. Chem., Stoechiom. Verwandtschaftsl. **92**, 129 (1917).
[29] N. Agmon and A. Szabo, J. Chem. Phys. **92**, 5270 (1990).
[30] S. A. Rice, *Diffusion-Limited Reactions* (Elsevier, Amsterdam, 1985).
[31] P. G. Wolynes and J. M. Deutch, J. Chem. Phys. **65**, 450 (1976).
[32] S. H. Northrup and J. T. Hynes, J. Chem. Phys. **71**, 871 (1979).
[33] R. C. Dorfman and M. D. Fayer, J. Chem. Phys. **96**, 7410 (1992).
[34] D. Rehm and A. Weller, Isr. J. Chem. **8**, 259 (1970).
[35] M. Chanon, M. D. Hawley, and M. A. Fox, in *Photoinduced Electron Transfer. Part A: Conceptual Basis*, edited by M. A. Fox and M. Chanon (Elsevier, New York, 1988), p. 1.
[36] J. Jortner, J. Chem. Phys. **64**, 4860 (1976).

[37] J. Jortner and M. Bixon, J. Chem. Phys. **88**, 167 (1988).
[38] J. R. Miller, J. V. Beitz, and R. K. Huddleston, J. Am. Chem. Soc. **106**, 5057 (1984).
[39] G. C. Walker, E. Akesson, A. E. Johnson, N. E. Levinger, and P. F. Barbara, J. Phys. Chem. **96**, 3728 (1992).
[40] J. A. Riddick, W. B. Bunger, and T. K. Sakano, *Organic Solvents: Physical Properties and Methods of Purification*, 4th ed. (Wiley, New York, 1986).
[41] A. Weller, Z. Phys. Chem., Neue Folge **133**, 93 (1982).
[42] T. Yamazaki, I. Yamazaki, and A. Osuka, J. Phys. Chem. B **102**, 7858 (1998).
[43] H. B. Gray and J. R. Winkler, Annu. Rev. Biochem. **65**, 537 (1996).
[44] G. L. Closs and J. R. Miller, Science **240**, 440 (1988).
[45] T. Guarr and G. McLendon, Coord. Chem. Rev. **68**, 1 (1985).
[46] R. P. Domingue and M. D. Fayer, J. Chem. Phys. **83**, 2242 (1985).